Synthesis and Mechanism of Spherical Ag-doped Polypyrrole Assisted by Complexing Agents

Chuanyun Wan (cywan@sit.edu.cn)
Shanghai Institute of Technology
Xiaoge Chen
Shanghai Institute of Technology
Xiya Liu
Shanghai Institute of Technology

Research Article

Keywords: spherical polypyrrole，Ag doping，micelle induction，formation mechanism

Posted Date: April 19th, 2021

DOI: https://doi.org/10.21203/rs.3.rs-389009/v1

Version of Record: A version of this preprint was published at Journal of Inorganic and Organometallic Polymers and Materials on November 12th, 2021. See the published version at https://doi.org/10.1007/s10904-021-02126-7.

Abstract

Highly dispersed Ag-doped PPy spherical composites can be efficiently synthesized visa oxidative polymerization of pyrrole with $FeCl_3$ in an aqueous Ag^+-containing solution in the presence of trisodium citrate, followed by concentrated ammonia treatment. However, the formation mechanisms involved in how to control the shape and how to get the metellic Ag^0 need further investigation. In order to elucidate the formation mechanisms, the intermediates in different reaction stage were collected and investigated. Combining the experimental phenomenon and the structure characterization of the samples, it was found that citrate ions make a role of complexing Ag^+ to produce $[Ag_3(C_6H_5O_7)_{n+1}]^{3n-}$ complexes in the early reaction stage, then mainly play a role of steric stabilizer of AgCl micelles and are responsible for the shape tailoring of PPy composite as well as the reduction of Ag^+ in the process of ammonia treatment. Evidently, negative-charged AgCl micelles become the main nucleation sites of pyrrole polymerization through the electrostatic attraction between the negative and positive ions. Concentrated ammonia is adopted to eliminate AgCl cores from the precursor of Ag-doped PPy composites obtained by chemical redox reaction and provides an accelerated reaction condition for reduction of Ag^+ by reductants (citrate ion or pyrrole monomer). Ag-containing micelles induction method is a facial chemical method to obtain uniform Ag-doped composites and can be broadened to design other Ag-containing functional materials.

1. Introduction

Silver one of the noble metals, owns excellent conductivity of heat and electricity, relatively low cost and fair stability in the ambient environment. In recent years, Ag nanostructures were widely investigated for their unique optical, electrical and chemical properties (Murphy, 2002; Hsu et al., 2007; Hou et al. 2013) in various fields including catalysts(Corro, et al., 2017; Sarma et al., 2017), optical devices (Sarma et al., 2018), optoelectronic devices(Monteiro et al., 2018), Surface Enhanced Raman Scattering (SERS)(Huang et al., 2018), therapeutic agent, etc.(Liu, 2018; Xu, 2020; Yuan et al., 2016). Hence, Ag nanostructures with different shapes (eg. nanowires (Chen et al., 2011; Caswell et al., 2003), nanospheres(Caswell et al., 2003; Chen et al., 2018) and different sizes (eg. nanometer([15] Misran, et al., 2018), micrometer(Chen et al., 2011) were designed separately or composed with other materials. In most cases, Ag nanostructures are applied by incorporating with functional material to enhance some special properties of these materials(Corro, et al., 2017; Sarma et al., 2017; Sarma et al., 2018; Monteiro et al., 2018; Huang et al., 2018; Yuan et al., 2016; Wan et al., 2014; Sawangphruk et al., 2012; Elsellami et al., 2017). For example, $Ag@SiO_2$ or $Ag@ZnO_2$ core-shell catalysts were prepared by reducing $AgNO_3$ impregnated on the surface of SiO_2 or ZnO powder and a good Diesel Particulate Matter (DPM) oxidation activity is obtained because of the presence of Ag^0 on the catalyst surfaces (Corro, et al., 2017). As an antibacterial agent, $Ag@Bi_2O_3$ nanocomposites were prepared by chemically precipitating Ag species on the surface of Bi_2O_3 nanospheres and displayed improved antibacterial ability in comparison with single component Bi_2O_3 nanospheres(Liu, 2018). TiO_2 is a popular functional material for its hydrophilic and depolluting properties. In order to improve TiO_2 photocatalytic activity, Ag-doped TiO_2 are also produced by

impregnating to TiO_2 solid nanomaterials in $AgNO_3$ solution(Elsellami et al., 2017). However, through impregnation or chemically deposition method, Ag species often tend to accumulate on the surface which a liquid can reach and is usually less in the interior of the materials, which is benefit to the interface reactions aimed on the surface of the materials.

In electrochemical application, Ag is also widely studied to dope the less-conductive active materials (MnO_2 (Wan et al., 2014; Sawangphruk et al., 2012), graphene(Sarno et al., 2018), $LiMn_2O_4$(Jiang et al., 2015), PPy (Yuan et al., 2016; Singu et al., 2018; Patil et al., 2013; Liu et al., 2013; Iqbal et al., 2020) to improve their electrochemical performance. In this case, the uniform distribution of Ag in the composite becomes very essential. Hence, in order to achieve the aim of uniform distribution of Ag in composite, different preparation methods and different preparation routes have been adopted(Corro, et al., 2017; Yuan et al., 2016; Caswell et al., 2003; Chen et al., 2018; Misran, et al., 2018; Wan et al., 2014; Sawangphruk et al., 2012; Elsellami et al., 2017; Sawangphruk et al., 2012; Sarno et al., 2018; Jiang et al., 2015) and chemical synthesis method is considered to be a more effective and easier way to modify the morphology and performance of the materials (Wan et al., 2014; Sawangphruk et al., 2012; Singu et al., 2018; Patil et al., 2013; Liu et al., 2013; Iqbal et al., 2020). Among of this, One-step in-situ synthesis of Ag-incorporated composite is very popular(Yuan et al., 2016; Wan et al., 2014; Sawangphruk et al., 2012; Sarno et al., 2018; Jiang et al., 2015; Iqbal et al., 2020; Feng et al., 2007; Singu et al., 2018). Therefore, PPy@Ag shell-core nanostructures were prepared by one-step interfacial polymerization for a dopamine biosensor (Feng et al., 2007). Spherical interlaced PPy/PAA/Ag composites, in which Ag nanoparticles attach onto the granules of polymer, were synthesized by chemical polymerization technique for supercapacitor (Patil et al., 2013). Recently, we reported Ag-doped submicron materials (Ag-doped MnO_2(Wan et al., 2014), Ag-PPy (Yuan et al., 2016) prepared by micelle-inducing chemical solution techniques. In our works, spherical structures are successfully synthesized and Ag species uniformly distribute in MnO_2 or PPy matrix, showing an improved electrochemical performance for supercapacitor. Pitifully, we didn't clearly elucidate the formation mechanism of spherical Ag-incorporated PPy or spherical Ag-doped MnO_2 except for reasonable reasoning in literatures (Yuan et al., 2016; Wan et al., 2014). Here, we synthesized spherical Ag-doped PPy composites visa oxidative polymerization of pyrrole with $FeCl_3$ in an aqueous Ag^+-containing solution assisted by trisodium citrate. The procedures of spherical Ag-doped PPy composites were studied in details and the formation mechanisms of spherical composites which included the role of all the materials and how to control spherical shape were also elucidated.

2. Experimental

Ag-incorporated PPy spherical composites were prepared by the same route recorded in reference (Yuan et al., 2016). Pyrrole (Py) monomer, silver nitrate ($AgNO_3$), trisodium citrate ($C_6H_5Na_3O_7 \cdot H_2O$) and ferric trichloride ($FeCl_3$) were used as the starting materials. The synthesis procedure of Ag-incorporated PPy composites can be divided into the following three steps. Step 1: 50 mL of a 0.07 mol L^{-1} trisodium citrate solution was dropped slowly into 200 mL of the colorless solution containing 0.015mol pyrrole monomer

and 0.0012 mol $AgNO_3$ at 0-2 ^{0}C and then stirred for 15min. White color appears initially when the droplets of trisodium citrate solution touch the surface of the solution and then vanishes gradually. A milk-like solution was obtained finally after stirring; step2: 50 mL of 1.0 mol L^{-1} ferric chloride solution was added dropwise to trigger the polymerization of pyrrole. In order to adjust the growth of PPy chains, the feeding speed of ferric chloride solution was controlled very slowly. With the increase of the in reaction time, the color of the solution changes from white to light green, dark green and finally black. The polymerization reaction was taken under constant stirring condition for approximately 10h. After polymerization, the black solid particles were collected by filtering the solution and completely washed with deionized water. The collected black solid powder is the precursor of spherical Ag-doped composite (coded as Ag/PPy-1); Step 3: the collected solid particles (Ag/PPy-1) were put into aqueous concentrated ammonia solution and stirred for 10min and then collected by filtration. This process was repeated twice and finally the solid residue was washed with deionized water or ethanol. The designed spherical Ag-incorporated PPy composite (codes as Ag/PPy-2) was obtained by filtering the residue followed by drying it in a vacuum oven at 80 ^{0}C for 12h.

X-ray diffraction (XRD) analysis was performed on an X-ray diffractometer (PAN alytical X'pert Pro, CuKα anode: λ=1.54187Å) to investigate the crystal structure of the samples. A scanning electron microscope (SEM, FEI NovaSEM ×30) and a transmission electron microscope (TEM Hitachi600) were used to examine the morphologies and structures of the samples. X-ray photoelectron spectroscopy (XPS VG ESCALAB 200i-XL) data were recorded with a Theta Probe electron spectrometer using A Kα (hv =1484.6eV) radiation. Spectral deconvolution was carried using a Gaussian-broadened Lorentzian curve-fitting program, and the binding energies were corrected by the C_{1s} line at 284.6 eV from adventitious carbon.

3. Results And Discussion

In the initial stage of the synthesis process, Ag^+ species are mixed with pyrrole. They can coexist together in reasonable short time because the weak oxidation ability to Pyrrole polymerization. Trisodium citrate is popular for the reduction and complexation for noble metal (eg. Ag or Au) (Feng et al., 2007; Dong et al., 2009; Ji et al., 2007; Yang et al., 2010). In step 1, when citrate ions is dropped into the Ag^+-containing solution, white color appears because $Ag_3C_6H_5O_7$ is formed according to the following reaction:

$$3Ag^+ + C_6H_5O_7^{3-} \longrightarrow Ag_3C_6H_5O_7 \downarrow \qquad (1)$$

Silver citrate is a white substance. It has a very limited solubility in water (the maximum concentration of silver ions in saturated solution of silver citrate in water is ca. 2.8×10^{-3} mol L^{-1}(Djokic, 2008). According to the amounts of the starting materials, the actual concentration of Ag^+ in solution is 4.8×10^{-3} mol L^{-1}, larger than the value of the maximum concentration of silver ions in a saturated aqueous solution. Hence, the precipitation of white $Ag_3C_6H_5O_7$ will occur. However, no white solid appeared on the bottom of the

reactor at the end of the step 1, indicating that the size of the obtained white powder is very small and reasonably stable in solution. It should thank to the existence of adequate citrate ions in reaction system. Compared to Ag ions (0.0012mol), the number of citrate ions (0.0035mol) which was afforded in solution is too adequate for the reaction (1). Hence, the surplus citrate ions will further react with silver citrate according to the following reaction (Ji et al., 2007):

$$Ag_3C_6H_5O_7 + n\ C_6H_5O_7^{3-} \longrightarrow [Ag_3 (C_6H_5O_7)_{n+1}]^{3n-} \qquad (2)$$

The obtained $[Ag_3(C_6H_5O_7)_{n+1}]^{3n-}$ complex ions are negative charged micelles, which are reasonably stable in solution. Till up to the step 1, the role of trisodium citrate should be the producer of negative-charged micelles, which can directionally induce the adsorption of cations (such as Fe^{3+}, the oxidant for pyrrole polymerization) around the micelles. The overall reaction for reaction 1 and reaction 2 can be written as the following reaction:

$$3Ag^+ + (n+1)\ C_6H_5O_7^{3-} \longrightarrow [Ag_3 (C_6H_5O_7)_{n+1}]^{3n-} \qquad (3)$$

The reaction (3) is reversible, depending on the concentrations of the involved species. Even though the complexation of citrate ions with Ag ions is predominant in this stage, the redox reaction between Ag^+ and citrate ions may occur according to the following reaction 4:

$$C_6H_5O_7^{3-} + 2Ag^+ \longrightarrow C_5H_4O_5^{2-} + H^+ + CO_2 + 2Ag^0 \qquad (4)$$

However, considering the mild reductive ability of citrate (Yang et al., 2010), this redox reaction rate is slow in present system and can be ignored in the initial synthesis stage. That is to say, at the end of the step 1, the reaction (3) is in a state of dynamically equilibrium in solution and $C_6H_5O_7^{3-}$ ions mainly serve as steric stabilizer of Ag^+-containing micelles.

In step 1, another reaction also exists in theory which is the reaction of the redox reaction of Ag^+ with pyrrole (reaction 5). However, the rate of this redox is also very low and the Ag-PPy nanoparticles was often obtained in condition of enough reaction time (several days(Dong et al., 2009), hence, reaction 5 can be disregarded in stage of step 1.

$$Py + Ag^+ \longrightarrow Py^+ + Ag^0 \qquad (5)$$

In step 2, a $FeCl_3$ solution was added dropwise to the system obtained by step 1, two kinds of reactions will occur in no doubt. As a strong oxidant, ferric ions will initiate the redox polymerization of pyrrole monomer as the following reaction:

$$Py + Fe^{3+} \longrightarrow Py^{+} + Fe^{2+} \qquad (6)$$

During Py polymerization, pyrrole initially loses one electron to be oxidized and then be followed by dimerization, aromation, oxidation of the dimer and finally realized the growth of PPy chains (Singu et al., 2018Genies et al., 1983). However, except for polymerization, the other reaction, almost simultaneously or even preferentially, is the reaction of chloride ions (Cl^-) with Ag^+ to produce AgCl when a droplet of $FeCl_3$ solution is dropped into the solution containing Ag^+ and pyrrole monomer (see reaction 7). With the increasing Cl^- ions, AgCl will continue to combine with Cl^- and become $AgCl_{x+1}^{x-}$ complexes (reaction 8).

$$Ag^{+} + Cl \longrightarrow AgCl \qquad (7)$$

$$AgCl + x\,Cl^{-} \longrightarrow [AgCl_{x+1}]^{x-} \qquad (8)$$

AgCl is also an insoluble white substance. The maximum concentration of Ag^+ in a saturated solution of AgCl in water is ca. 1.3×10^{-5} mol L^{-1} (this value can further decrease when the water is substituted to other organic solvent) (Chen et al., 2018), much lower than that of Ag^+ concentration of $Ag_3C_6H_5O_7$ saturated aqueous solution. Hence, when $FeCl_3$ is introduced into the solution obtained in step 1, evidently, the reverse reaction of reaction (3) will occur because of the competition of the reaction (7) and (8). In this case, the negative charged $[AgCl_{x+1}]^{x-}$ complex and the negative charged $[Ag_3\ (C_6H_5O_7)_{n+1}]^{3n-}$ complex coexist in the solution and they both have the ability of adsorbing positive charge Fe^{3+} from the solution because of the electrostatic attraction of the negative and positive ions. Hence, the polymerization of Py will preferentially occur on the surfaces of negative charged complex micelles, which become the nucleation sites of PPy polymerization. In order to verify this speculation, the black solid product from step 2 was collected by filtration and washed completely with deionized water for several times until the filtrate was clear and colorless. The black solid powder (named PPy-Ag-1) was obtained after drying the washed residue in a vacuum oven.

The color of the obtained powder indicates that PPy was obtained successfully because only PPy is black among the possible products. The powder X-ray diffraction (XRD) patterns were applied to detect the crystal structure of the sample. The XRD patterns of PPy-Ag-1 shown in Fig.1, is clearly shown that there are several strong peaks. The peaks at $2\theta = 27.8^0$, 32.2^0, 46.2^0, 54.8^0, 57.5^0, 67.5^0, 74.5^0 and 76.7^0 are completely in accordance with the reported data for AgCl and can be assigned to the diffraction from the (111), (200), (220), (311), (222), (400), (331) and (420) planes (JCPDS 31-1238), indicating the presence of crystallic AgCl in PPy-Ag-1 sample. No detectable $Ag_3C_6H_5O_7$ exists in sample. The loss of $Ag_3C_6H_5O_7$ evidently verifies the reaction (7) preferentially take place in solution system and hence, negative charged $[AgCl_{x+1}]^{x-}$ complexes surely become the main micelles for induction nucleation of PPy in step 2. From the XRD patterns, it is failure to distinguish the PPy structure because it is amorphous (the XRD patterns of PPy is also shown in Fig.1 for comparison). In spite that Ag-incorporated PPy has been

successfully produced (Yuan et al., 2016), however, metallic Ag, which is supposed to be obtained through the reaction (4) and (5) in step 2, is not visible in PPy-Ag-1 sample according to the results of XRD tests.

XPS spectra were obtained in order to elucidate both the elemental components and chemical state of the elements of the samples. Fig.2a show the survey scan spectra of PPy-Ag-1 sample and pure PPy. New peaks at ca. 370 eV, attributing to Ag_{3d} binding energy, were observed significantly in PPy-Ag-1 spectrum, suggesting the present of Ag species in the sample. This result is in accordance with the XRD measurement. However, the high-resolution Ag_{3d} spectrum of PPy-Ag-1shown in Fig. 2b, indicates that the $Ag_{3d5/2}$ is at 368.25 eV while the $Ag_{3d3/2}$ is 374.25 eV, which is apparently corresponding to Ag^0 electronic state (Yuan et al., 2016; Misran, et al., 2018; Prieto et al., 2012). It is inconceivable that the information of Ag^+ is absent in XPS spectra. The contradiction between the XPS tests and the XRD tests can be considered from the difference between their individual detection mechanisms. The XPS test preferentially detects the element information from the thinner surface (2-10nm) and the X-ray in XRD test can penetrate to the micron depth of the sample and catch the element information. Meanwhile, the detection limit of the XPS test (0.1-1 at. %) is much lower than that of the XRD test (~2%) (Perry et al., 1983; Zhang et al., 1999). If the hypothesis of micelle-inducing nucleation of PPy is correct, the insoluble AgCls must be covered by PPy and locate in the center of the PPy-Ag-1. Hence, the information of Ag^+ species is failure to be detected by XPS because of the long distance of AgCl to the surface of the sample. The loss of the Ag^0 species in XRD tests may be due to its low quantity in PPy-Ag-1, indicating that the reaction (4) and (5) take place at a very low reaction rate.

In order to verify the hypothesis of micelle-induction nucleation, PPy-Ag-1 sample as well as pure PPy (without $AgNO_3$ in solution) was obtained for comparison at the stage of step 2. Their morphologies were observed by Scanning electron microscopy (SEM) and transmission electron microscopy (TEM) and shown in Fig.3. A bright spot in the center of the PPy-Ag-1 particle (Fig.3c) can be clearly observed, suggesting that the obtained PPy-Ag-1 is a heterogeneous structure compared to pure PPy particles. The TEM image of PPy-Ag-1 furtherly confirms the core-shell structure of PPy-Ag-1. Obviously, the core of PPy-Ag-1 is AgCl nanograins which have been detected by the XRD tests. The morphology measurements of PPy-Ag-1 verify the function of micelle-induction for tailoring the shape of PPy and AgCl micelles play a main role of the template as nucleation sites of PPy spherical structure.

However, the AgCl-containing PPy-Ag-1 is not the desired product. In order to get pure Ag-doped PPy composite, AgCl nanograins have to be eliminated from the PPy-Ag-1. In step 3, ammonia was applied to treat the PPy-Ag-1 powders for several times and then the residue was collected by filtration and washed completely with deionized water followed by drying in a vacuum condition. The obtained powder was coded as PPy-Ag-2. The XRD patterns of PPy-Ag-2 was collected and shown in Fig.4. It is very interesting that several strong diffraction peaks which are completely different from that of AgCl appear at $2\theta = 38.1^0$, 44.3^0, 64.5^0, and 77.3^0, corresponding to the (111), (200), (220) and (311) planes of face-centered cubic structure of silver (JCPDS 04-0783) (Yuan et al., 2016; Chen et al., 2018). This result indicates that

AgCl has been removed from the PPy-Ag-1 sample and a larger amount of Ag^0 is produced after treating PPy-Ag-1with concentrated ammonia. Fig.5 presents the images of the morphology of PPy-Ag-2. After treatment by concentrated ammonia, the spherical particles of PPy-Ag-1 remain spherical morphology (Fig.5a) and the cores located in the powder disappear. The TEM image of the obtained PPy-Ag-2 spherical structure is hollow, evidently verifying that AgCl nanograins located in the center of the PPy-Ag-1 is successfully etched by ammonia. So, the following reaction is supposed to occur in the third step:

$$AgCl + 2\ NH_4OH \longrightarrow [Ag(NH_3)_2]^+ + Cl + 2\ H_2O \qquad (9)$$

In strong basic solution of ammonia, AgCl will react with ammonia to produce water soluble $[Ag(NH_3)_2]^+$ complex and is dissolved into the water from the insoluble PPy matrix.

Though the reaction (9) reasonably gives the elucidation of AgCl how to eliminate from the powder, another interesting phenomenon should not be ignored. Different from the PPy-Ag-1 sample, Ag^0 is obviously detected by XRD measurement, indicating that the larger number of Ag^0 is produced by ammonia treatment. The increase of Ag^0 in PPy-Ag composite is surely due to the reduction of Ag^+ ions which are incorporated in the composite matrix. Except for Ag reduction due to light irradiation or other unidentified factors, the $Ag_3C_6H_5O_7$ is the species which can be firstly considered because it provides not only Ag^+ ions, but also $C_6H_5O_7^{3-}$, the reductant of Ag^+. In fact, for PPy-Ag-1, $Ag_3C_6H_5O_7$ is inevitably inlayed into the composite matrix for the complexion of $C_6H_5O_7^{3-}$ with Ag^+. As described before, citrate ion is a mild reductant for Ag^+ and in order to accelerate the reduction reaction, heat-treatment techniques are often applied(Ji et al., 2007; Pong et al., 2007). This condition doesn't be afforded to realize the redox reaction in our study. However, it is reported that the rate of citrate reduction of Ag^+ depends on the pH value of the reaction and higher pH can promote the reductive ability of citrate (Dong et al., 2009). Hence, the increase of Ag^0 in PPy-Ag composite after ammonia treatment may be due to the occurence of the reaction (4) because the pH value of concentrated ammonia is very high. Based on the above discussion, concentrated ammonia plays two main roles in system. One function of ammonia is dissolving AgCl to remove the micelle template. The other is accelerating the citrate reduction of Ag^+. As for citrate ions, they play roles of Ag^+ reservoir in the form of $[Ag_3\ (C_6H_5O_7)_{n+1}]^{3n-}$ as well as the reductant of Ag^+. Except for this, they are also responsible for the spherical structure of PPy-Ag composite (Yuan et al., 2016). The function of citrate will be elucidated in more details in the following study.

In order to further explore the function of citrate in spherical Ag-incorporated PPy composite, Ag-doped PPy particles were prepared in solution without citrate ions for comparison. The solid powders without treated by ammonia are collected and named as PPy-Ag-1'. PPy-Ag-2' representes the product washed by ammonia. The TEM image of PPy-Ag-1' shown in Fig.6a clearly reveals that the AgCl cores exist in the obtained samples and the hollows are left in PPy-Ag-2' powder (Fig.6b) after treating the sample PPy-Ag-1' with concentrated ammonia, indicating the evident induction nucleation of AgCl micelles for Py polymerization in the condition of the absence of citrate ions. Unfortunately, in the absence of citrate

ions, the obtained PPy-Ag-1’ grains aggregate together and the shape of the powder is not a single sphere. Moreover, there often exists more than one AgCl nucleus in the large PPy-Ag powder, suggesting the weak steric affection of AgCl micelles. The single spherical composite obtained from the system containing citrate ions indicates that citrate ions improve the effect of steric stabilization of AgCl micelles and the shape of the product can be tailored by changing the molar ratio of Ag^+ to citrate ion (Yuan et al., 2016).

The XRD patterns of PPy-Ag-1’ and PPy-Ag-2’ which are obtained in the solution without citrate ions are recorded and shown in Fig.7. The result is the same to that of samples obtained from the solution containing citrate ions. Before washed by ammonia, the sample named PPy-Ag-1’ contains AgCl and has no visible metallic Ag^0. After treated by concentrated ammonia, Ag^0 is visible in PPy-Ag-2’ sample, indicating that a base intensifies the reduction reaction of Ag^+ to produce Ag^0, which should correspond to the reaction (5). That is to say, there are some amount of invisible Ag^+ and unoxidized Pyrrole in the PPy-Ag-1’matrix and the inlayed Ag^+ species will react with pyrrole monomer to produce Ag^0 in high pH condition. The reaction (5) may also exist in process of PPy-Ag-2 preparation.

The XPS Ag_{3d} spectra of Ag-doped PPy composite prepared in absence of citrate ions is compared to that of Ag-doped PPy composite obtained in condition of containing citrate ions. As shown in Fig.8, there is no obvious difference between them, indicating that Ag-doped PPy composite can be successfully synthesized whether the citrate ions exist or not. Even though this, the Ag content of PPy-Ag-2, synthesize from the solution containing citrate ions is 0.93 at. %, is higher than that of PPy-Ag-2’(0.73 at.%) obtained from the solution in absence of citrate ions. The increase of Ag content in sample reveals that citrate ion can more efficiently lock Ag^+ into solid PPy matrix because of the formation of $Ag_3C_6H_5O_7$ micelle in solution. Hence, the reaction (4) and (5) are both responsible for the increase of the amount of Ag^0 in PPy-Ag-2.

According to the above process analysis, the formation of spherical Ag-doped polypyrrole visa oxidative polymerization of pyrrole with $FeCl_3$ in an aqueous Ag^+-containing solution in the presence of trisodium citrate are clear. As Ag^+ complexing agent, $C_6H_5O_7^{3-}$ species complex Ag^+ and form soluble Ag complexes (the reaction 1 and 2). The reversible equilibrium of the reaction 3 will adjust the free Ag^+ concentration in solution. The reduction of Ag^+ by $C_6H_5O_7^{3-}$ species is slow but can occur at reasonable condition. When $FeCl_3$ species add to the solution, the redox polymerization of pyrrole monomer occur quickly for the strong oxidation of Fe^{3+} ions (the reaction 6). Meanwhile, chloride ions (Cl^-) from $FeCl_3$ will react with free Ag^+ to produce AgCl (the reaction 7) and make the reversible reaction of the reaction 3 occur. With the increase of $FeCl_3$ in solution, pyrrole monomer continues to be oxidized to form PPy and AgCl will continue combine with the increasing Cl^- ions and become negative charged $AgCl_{x+1}^{x-}$ micelles (the reaction 8). The negative charged AgCl micelles will play the active sites of PPy crystallization growth and make the PPy spherical. When the size of AgCl is enough large, it can be clearly detected (Fig.6). Sometimes, it is invisible for its too small size(Yuan et al., 2016). The complexion of $C_6H_5O_7^{3-}$

species with Ag^+ can adjust the amount of free Ag^+ in solution as well as the particle dispersion of PPy(Fig.3). With the increase of reaction time, Ag^+ combined with $C_6H_5O_7^{3-}$ will dissolute and be combined with Cl^- for the stronger complexing ability of Cl^- compared to $C_6H_5O_7^{3-}$. A dynamic balance will occur. Hence, insoluble AgCl and $Ag_3C_6H_5O_7$ are expected to coexist in PPy matrix. It is normal the AgCl can be detected in water-washed PPy sample (Fig.4 and Fig.7). In order to remove the AgCl or $Ag_3C_6H_5O_7$, ammonia was used to wash the obtained sample. It is obvious that the black cores in spherical sample disappear because of the reaction 9. During the reaction, a portion of Ag^+ will transferred to metallic Ag due to light irradiation or other unidentified factors. Ag-doped PPy or MnO_2 have been successfully obtained(Yuan et al., 2016; Wan et al., 2014). However, when $C_6H_5O_7^{3-}$ species are used to complex Ag^+, the content of Ag in PPy is little higher than that of no $C_6H_5O_7^{3-}$ species. It may be the reason that $Ag_3C_6H_5O_7$ nanoparticle coexist in PPy matrix and the improved reduction ability of $C_6H_5O_7^{3-}$ species make more Ag^+ reduce to Ag^0 in alkali condition. The whole formation mechanism of spherical Ag-doped PPy assisted by complexing agents can be illustrated by the flow chart shown in Fig.9.

4. Conclusions

Spherical Ag-doped PPy composites were synthesized firstly using chemical redox reaction in solution containing pyrrole monomer, $AgNO_3$, trisodium citrate and $FeCl_3$ and then treating the solid product with ammonia. In order to elucidate the formation mechanisms of Ag doping and spherical shape of PPy, the intermediates in different reaction stage was collected and characterized with XRD measurement, SEM and TEM microscopy and XPS scanning spectrum. The experimental phenomenon and the physical characterization of the samples collected in different reaction stage indicate that citrate ions make a role of complexing Ag^+ to produce $[Ag_3(C_6H_5O_7)_{n+1}]^{3n-}$ complexes in the initial reaction stage, then $[Ag_3(C_6H_5O_7)_{n+1}]^{3n-}$ complexes act as a reservoir of Ag^+. In the following reaction stage, citrate ions also play a role of a steric stabilizer of AgCl micelles in whole reaction and are responsible for the shape tailoring of PPy composites as well as the reduction of Ag^+. Evidently, negative-charged AgCl micelles induce nucleation of pyrrole polymerization through electrostatic attraction of the negative and positive ions and become the core of spherical Ag-doped PPy composites. Concentrated ammonia efficiently eliminates AgCl micelles from the solid residue obtained from chemical redox reaction and provides an accelerated reaction condition for reduction of Ag^+ by reductants (citrate ion or pyrrole monomer). Ag-containing micelles induction method is a facial chemical method to obtain uniform Ag-doped composites and can be broadened to design other Ag-containing functional materials.

Declarations

This study was funded by authors themselves. The authors declare that they have no conflict of interest.

References

[1] Murphy CJ (2002). Nanocubes and Nanoboxes. Science, 298: 2139-2141. doi: 10.1126/science.1080007.

[2] Hsu SLC, Wu RT (2007). Synthesis of contamination-free silver nanoparticle suspension for micro-interconnects. Mater. Lett., 61(17): 3719-3722. doi: 10.1016/j.matlet.2006.12.040

[3] Hou S, Hu XN, Wen T, Liu WQ, Wu XC (2013). Core-shell noble metal nanostructures templated by gold nanorods. Adv. Mater., 25(28): 3857-3862. doi: 10.1002/adma.201301169.

[4] Corro G, Vidal E, Cebada S, Pal U, Banuelos F, Vargas D, Guilleminot E (2017). Electronic state of silver in Ag/SiO_2 and Ag/ZnO catalysts and its effect on diesel particulate matter oxidation: An XPS study. Appl. Catal. B: Environmental. 216: 1-10. doi: 10.1016/j.apcatb.2017.05.059

[5] Sarma B, Sarma BK (2017). Fabrication of Ag/ZnO heterostructure and the role of surface coverage of ZnO microrods by Ag nanoparticles on the photophysical and photocatalytic properties of the metal-semiconductor system. Appl. Surf. Sci. 410:557-565. doi.: 10.1016/j.apsusc.2017.03.154.

[6] Sarma B, Sarma BK (2018). Role of residual stress and texture of ZnO nanocrystals on electro-optical properites of ZnO/Ag/ZnO multilayer transparent conductors. J. Alloy. Compd., 734: 210-219. doi: 10.1016/j.jallcom.2017.11.028.

[7] Monteiro JFHL, Monteiro FC, Jurelo AR, Mosca DH (2018). Conductivity In (Ag, Mg)-doped delafossite oxide $CuCrO_2$. Ceram. Int., 44(12): 14101-14107. doi: 10.1016/j.ceramint.2018.05.008.

[8] Huang QL, Wei WX, Wang LL, Chen HB, Li T, Zhu XS, Wu YP (2018). Synthesis of uniform Ag nanosponges and its SERS application. Spectrochim. Acta A: Mol. Biomol. Spectrosc., 201: 300-305. doi: 10.1016/j.saa.2018.05.019.

[9] Liu Q, Ju L, Zhong X, Dai Z, Lu Z, Yang H, Chen R (2018). Enhanced antibacterial activity and mechanism studies of Ag/Bi_2O_3 nanocomposites. Adv. Powder Technol., 29(9): 2082-2090. doi: 10.1016/j.apt.2018.05.015.

[10] Xu Y, Ma JX, Han Y, Xu HB, Wang Y, Qi DP, Wang W (2020). A simple and universal strategy to deposit Ag/polypyrrole on various substrates for enhanced interfacial solar evaporation and antibacterial activity. Chem. Eng. J. 384: 123379-123387. doi: 10.1016/j.cej.2019.123379.

[11] Yuan LY, Wan CY, Ye XR. Wu FH (2016). Facial synthesis of silver-incorporated conductive polypyrrole submicron spheres for supercapacitors. Electrochim. Acta. 213: 115-123. doi: 10.1016/j.electacta.2016.06.165.

[12] Chen DP, Qiao XL, Qiu XL, Chen JG, Jiang RZ (2011). Large-scale synthesis of silver nanowires via a solvothermal method. J. Mater. Sci.: Mater. Electron. 22: 6-13. doi.: 10.1007/s10854-010-0074-2.

[13] Caswell KK, Bender CM, Murphy CJ (2003). Seedless, surfactantless wet chemical synthesis of silver nanowires. Nano Letters. 3(5): 667-669. doi.: 10.1021/nl0341178.

[14] Chen SY, Carey III JL, Whitcomb DR, Buhlmann P, Penn RL (2018). Elucidating the role of AgCl in the nucleation and growth of silver nanoparticles in ethylene glycol. Cryst. Growth Des., 18(1): 324-330. doi.: 10.1021/acs.cgd.7b01300.

[15] Misran H, Salim MA, Ramesh S (2018), Effect of Ag nanoparticles seeding on the properties of silica spheres. Ceram. Int., 44(6): 5901-5908. doi.: 10.1016/j.ceramint.2017.12.118.

[16] Wan CY, Yuan LY, Ye XR, Wu FH (2014). Silver chloride micelle-induced tuning of pseudocapacitive manganese dioxide. Electrochim. Acta, 147: 712-719. doi: 10.1016/j.electacta.2014.10.013.

[17] Sawangphruk M, Kaewsongpol T. Direct electrodeposition and superior pseudocapacitive property of ultrahigh porous silver-incorporated polyaniline films. Mater. Lett. 87: 142-145. doi.: 10.1016/j.matlet.2012.07.103

[18] Elsellami L, Dappozze F, Houas A, Guillard C. (2017). Effect of Ag^{+} reduction on the photocatalytic activity of Ag-doped TiO_2. *Superlatt. Microstruc*t. 109: 511-518. doi: 10.1016/j.spmi.2017.05.043.

[19] Sawangphruk M, Pinitsoontorn S, Limtrakul J (2012). Surfactant-assisted electrodeposition and improved electrochemical capacitance of silver-doped manganese oxide pseudocapacitor electrodes. J. Solid State Electrochem. 16: 2623-2629. doi: 10.1007/s10008-012-1691-x.

[20] Sarno M, Casa M (2018). Green and one-step synthesis for Ag/graphene hybrid supercapacitor with remarkable performance. J. Phys. Chem. Solids. 120: 241-249. doi: 10.1016/j.jpcs.2018.04.045.

[21] Jiang RY, Cui CY, Ma HY, Ma HF, Chen T (2015). Study on the enhanced electrochemical performance of $LiMn_2O_4$ cathode material at 55 ^{0}C by the nano Ag-coating. J. Electroanal. Chem. 744: 69-76. doi: 10.1016/j.jelechem.2015.02.016.

[22] Singu BS, Yoon KR (2018). Highly exfoliated GO-PPy-Ag ternary nanocomposite for electrochemical supercapacitor. Electrochim. Acta. 268: 304-315. doi: 10.1016/j.electacta.2018.02.076.

[23] Patil DS, Pawar SA, Devan RS, Gang MG, Ma YR, Kim JH, Tatil PS (2013). Electrochemical supercapacitor electrode material based on polyacrylic acid/polypyrrole/silver composite. Electrochim. Acta. 105: 569-577. doi.: 10.1016/j.electacta.2013.05.022.

[24] Liu J, Li M, Zhang YQ, Yang LL, Yao JS (2013). Preparation and enhanced electrochemical properties of Ag/polypyrrole composites electrode materials. J. Appl. Polym. Sci. 129: 3787-3792. doi.: 10.1002/app.39102.

[25] Iqbal J, Numan A, Ansari MO, Jagadish PR, Jafer R, Bashir S, Mohamad S, Ramesh K, Ramesh S (2020). Facile synthesis of ternary nanocomposite of polypyrrole incorporated with cobalt oxide and

silver nanoparticles for high performance supercapattery. Electrochim. Acta 348: 136313-136322. doi: 10.1016/j.electacta.2020.136313.

[26] Feng XM, Huang HP, Ye QQ, Zhu JJ, Hou WH (2007). Ag/Polypyrrole core-shell nanostructures: interface polymerization, characterization, and modification by gold nanoparticles. J. Phys. Chem. C 111(24): 8463-8468. doi: 10.1021/jp071140z.

[27] Singu BS, Yoon KR (2018). Mesoporous polypyrrole-Ag nanocomposite for supercapacitors. J. Alloy. Compd., 742: 610-618. doi: 10.1016/j.jallcom.2018.01.328.

[28] Dong XY, Ji XH, Wu HL, Zhao LL, Li J, Yang WS (2009). Shape control of silver nanoparticles by stepwise citrate reduction. J. Phys. Chem., 113(16): 6573-6576. doi: 10.1021/jp900775b.

[29] Ji XH, Song XN, Li J., Bai YB, Yang WS, Peng XG (2007). Size control of gold nanocrystals in citrate reduction: the third role of citrate. J. Am. Chem. Soc., 129(45): 13939-13948. doi: 10.1021/ja074447k.

[30] Yang ZQ, Qian HJ, Chen HY, Anker JN (2010). One-pot hydrothermal synthesis of silver nanowires via citrate reduction. J. Colloid Interface Sci. 352(2): 285-291. doi: 10.1016/j.jcis.2010.08.072.

[31] Djokic S (2008). Synthesis and antimicrobial activity of silver citrate complexes. Bioinorg. Chem. Appl., 2008: 1-7. doi:10.1155/2008/436458.

[32] Genies EM, Bidan G, Diaz AF (1983). Spectroelectrochemical study of polypyrrole films. J. Electroanal. Chem. 149(1-2): 101-103. doi: 10.1016/s0022-0728(83)80561-0.

[33] Prieto P, Nistor V, Nouneh K, Oyama M, Abd-Lefdil M, Diaz R (2012). XPS study of silver, nickel and bimetallic silver-nickel nanoparticles prepared by seed-mediated growth. Appl. Surf. Sci. 258(22): 8807-8813. doi: 10.1016/j.apsusc.2012.05.095.

[34] Perry DL, Grint A (1983). Application of XPS to coal characterization. Fuel, 62(9): 1024-1033. doi: 10.1016/0016-2361(83)90135-7.

[35] Zhang S, Xie H, Zeng XT, Hing R (1999). Residual stress characterization of diamond-like carbon coatings by an X-ray diffraction method. Surf. Coat. Technol. 122(2-3): 219-224. doi: 10.1016/S0257-8972(99)00298-4.

[36] Pong BK, Elim HI, Chong JX, Ji W, Trout BL, Lee JY (2007). New insights on the nanoparticle growth mechanism in the citrate reduction of gold(III) salt: formation of the Au nanowire intermediate and its nonlinear optical properties. J. Phys. Chem. C, 2007, 111: 6281–6287. doi: 10.1021/jp068666o.

Figures

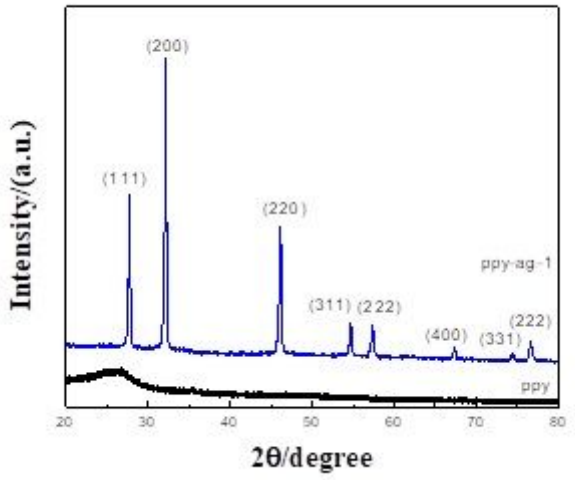

Figure 1

XRD patterns of PPy-Ag-1 and pure PPy.

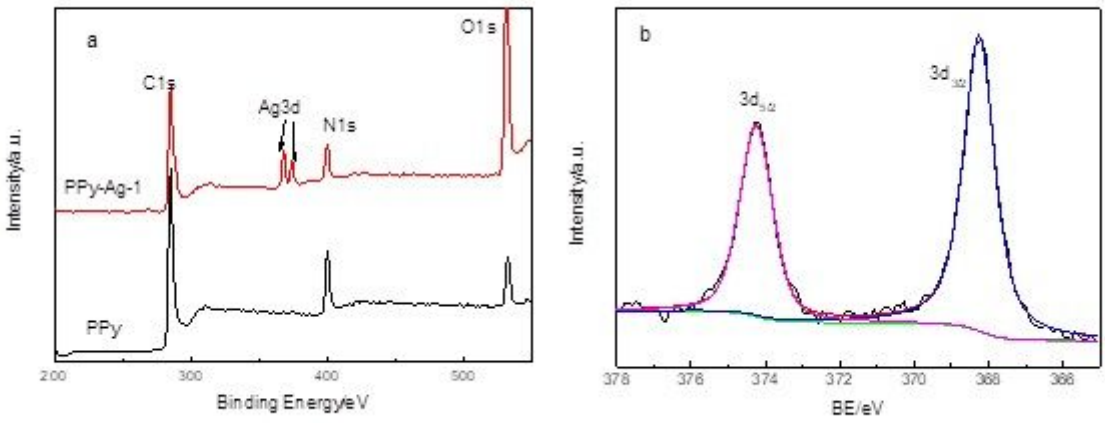

Figure 2

XPS survey scan spectra (a) and narrow scan at Ag3d orbit (b) of PPy-Ag-1.

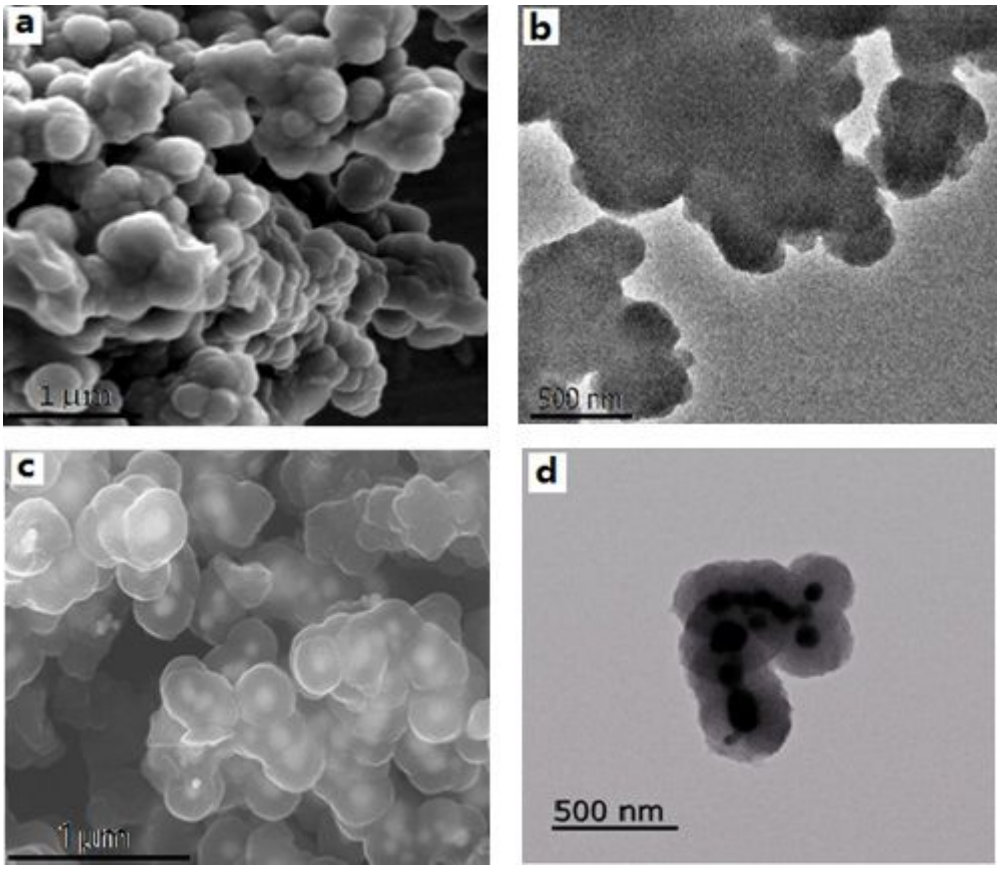

Figure 3

SEM images(a,c) and TEM images (b,d) of PPy(a,b) and PPy-Ag-1(c,d).

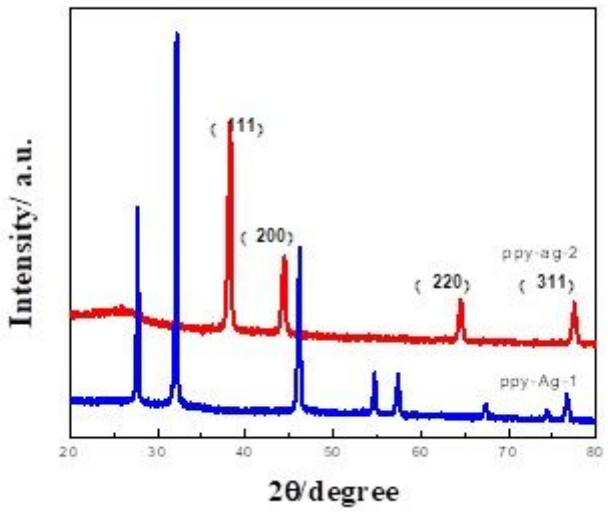

Figure 4

XRD patterns of PPy-Ag-2 and PPy-Ag-1.

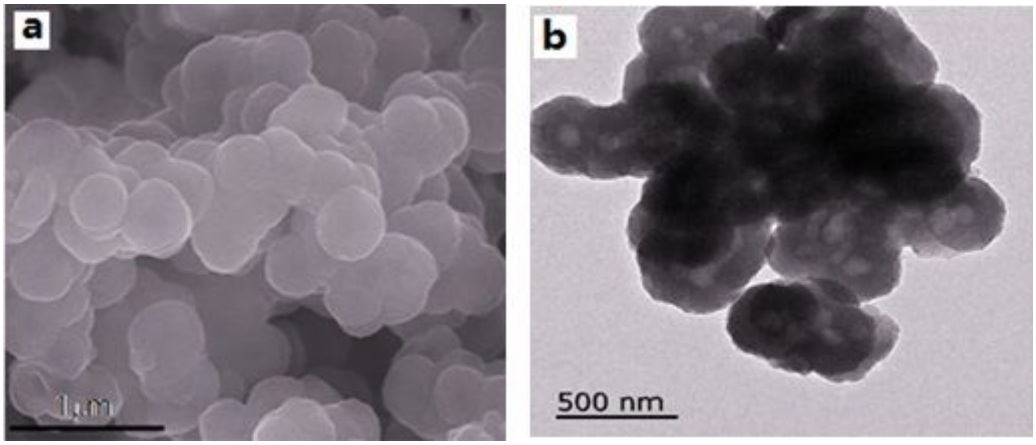

Figure 5

SEM image (a) and TEM image (b) of PPy-Ag-2.

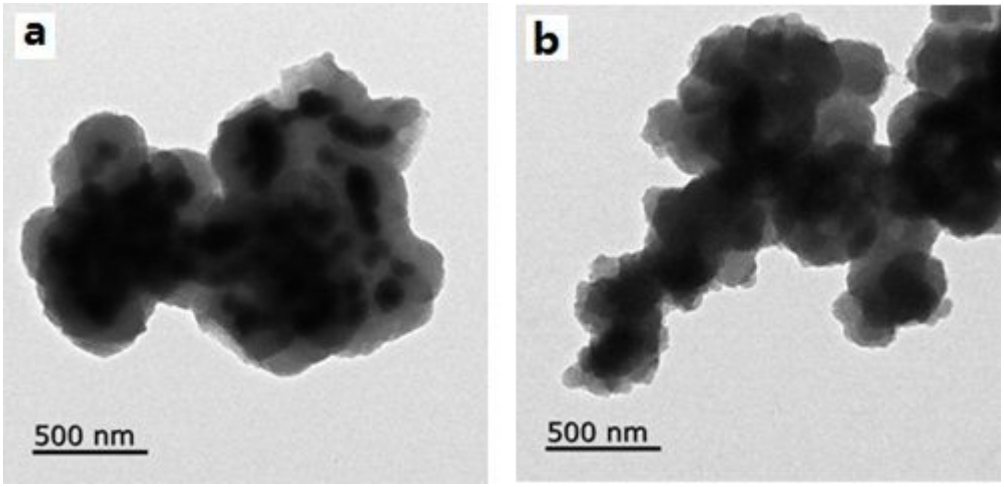

Figure 6

TEM images of PPy-Ag-1’ (a) and PPy-Ag-2’(b).

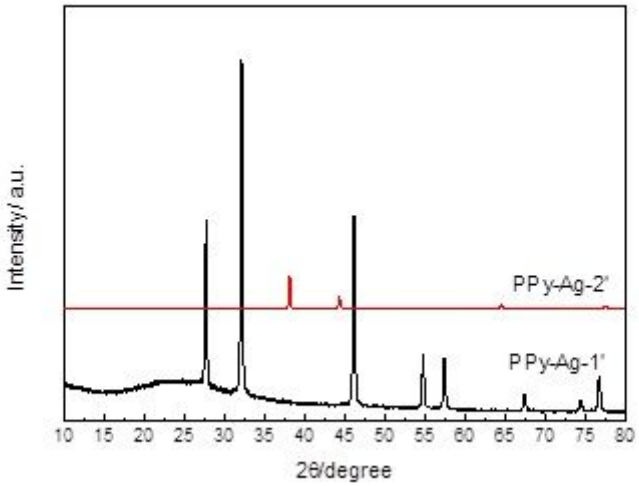

Figure 7

XRD patterns of PPy-Ag-2’ and PPy-Ag-1’.

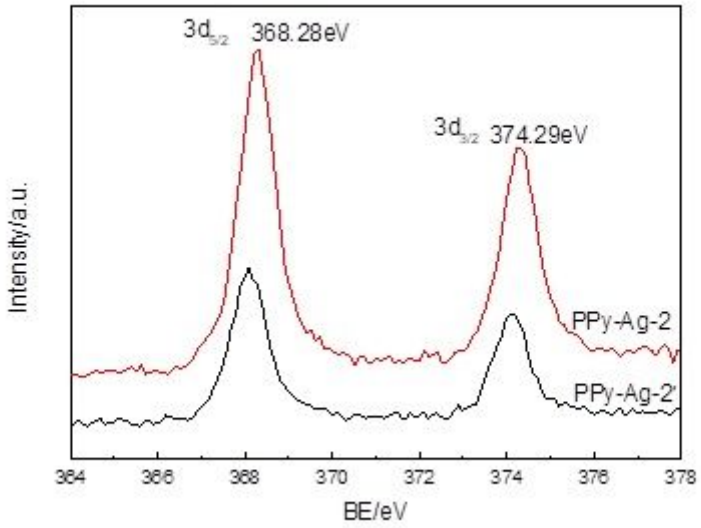

Figure 8

High-resolution Ag3d XPS spectra for Ag-doped PPy composite. (a) PPy-Ag-2; (b) PPy-Ag-2’.

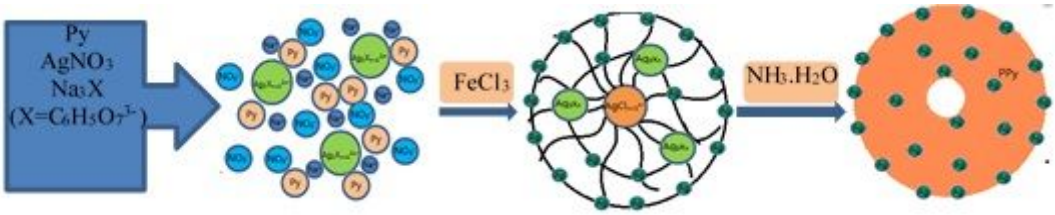

Figure 9

Formation mechanism Schematic diagram of spherical Ag-doped PPy assisted by complexing agents.